Medical Physics
The International Journal of Medical Physics Research and Practice

Respiration-phase-matched digital tomosynthesis imaging for moving target verification: A feasibility study

You Zhang, Lei Ren, C. Clifton Ling, and Fang-Fang Yin

Citation: Medical Physics **40**, 071723 (2013); doi: 10.1118/1.4810921
View online: http://dx.doi.org/10.1118/1.4810921
View Table of Contents: http://scitation.aip.org/content/aapm/journal/medphys/40/7?ver=pdfcov
Published by the American Association of Physicists in Medicine

Respiration-phase-matched digital tomosynthesis imaging for moving target verification: A feasibility study

You Zhang[a)]
Medical Physics Graduate Program, Duke University, Durham, North Carolina 27710

Lei Ren
Medical Physics Graduate Program, Duke University, Durham, North Carolina 27710 and Department of Radiation Oncology, Duke University Medical Center, Durham, North Carolina 27710

C. Clifton Ling
Varian Medical Systems, Inc., Palo Alto, California 94304; Department of Radiation Oncology, Stanford University School of Medicine, Stanford, California 94305; and Memorial Sloan-Kettering Cancer Center (Emeritus), New York, New York 10065

Fang-Fang Yin
Medical Physics Graduate Program, Duke University, Durham, North Carolina 27710 and Department of Radiation Oncology, Duke University Medical Center, Durham, North Carolina 27710

(Received 26 December 2012; revised 14 May 2013; accepted for publication 14 May 2013; published 20 June 2013)

Purpose: To develop a respiration-phase-matched digital tomosynthesis (DTS) technique to monitor moving targets, and to evaluate its accuracy for various imaging parameters and anatomical characteristics.
Methods: Previously developed 3D-DTS techniques, registering onboard DTS (OB-DTS, reconstructed from onboard projections) to reference DTS (R-DTS, reconstructed from DRRs of 3D reference CT), are inadequate to monitor moving targets. The authors' proposed respiration-phase-matched DTS technique registers OB-DTS to R-DTS reconstructed from DRRs generated by the same phase images of 4D reference CT as the corresponding onboard projections. To evaluate the improved accuracy of the author's technique, the authors performed thoracic phantom studies using (1) simulation with the 4D digital extended-cardiac-torso (XCAT) phantom, and (2) experiments with an anthropomorphic motion phantom. The studies were performed for various: respiratory cycle (RC), scan angle, and fraction of RC contained therein. Also, the authors assessed the accuracy of their technique relative to target size/location, and respiration inconsistencies from the R-DTS to OB-DTS.
Results: In both simulation and experimental studies, the respiration-phase-matched DTS technique is significantly more accurate in determining moving target positions. For 324 different scenarios simulated by XCAT, the respiration-phase-matched DTS technique localizes the 3D target position to errors of 1.07 ± 0.57 mm (mean $\pm$ S.D.), as compared to (a) 2.58 ± 1.37 and (b) 7.37 ± 4.18 mm, for 3D-DTS using 3D reference CT of (a) average intensity projection and (b) free-breathing CT. For 60 scenarios evaluated through experimental study, the uncertainties corresponding to those above are 1.24 ± 0.87, 2.42 ± 1.80, and 5.77 ± 6.45 mm, respectively. For a given scan angle, the accuracy of respiration-phase-matched DTS technique is less dependent on RC and the fraction of RC included in the scan. Increasing scan angle improves its accuracy. For different target locations, the targets near the chest wall or in the middle of lung provide higher registration accuracy compared to those near the mediastinum and diaphragm. Larger targets provide higher registration accuracy than small targets. Different respiratory cycle inconsistencies from R-DTS to OB-DTS minimally affect the registration accuracy. Increasing the respiratory amplitude inconsistencies will decrease the accuracy.
Conclusions: The respiration-phase-matched DTS is more accurate and robust in determining moving target positions than 3D-DTS. It has potential application in pretreatment setup, post-treatment analysis, and intrafractional target verification. © *2013 American Association of Physicists in Medicine*. [http://dx.doi.org/10.1118/1.4810921]

Key words: digital tomosynthesis, phase-matched, target motion, image registration, respiratory inconsistency

I. INTRODUCTION

Modern radiotherapy treatment techniques, such as intensity-modulated radiation therapy (IMRT) (Ref. 1) and volumetric modulated arc therapy (VMAT),[2] produce highly conformal coverage of the planning target volume (PTV) with steep dose gradient to spare the adjacent normal tissues. These features, however, also increase the probability of marginal miss and

motivated the development of image-guided radiation therapy (IGRT).[3] To localize the target before treatment, and verify its position during treatment, a number of methods have been developed and implemented, such as 2D radiography, 3D cone-beam CT (CBCT), or Calypso GPS tracking (Calypso, Seattle, WA).[4–12]

Besides these techniques, digital tomosynthesis (DTS) is a noninvasive imaging technique[13–16] which provides pseudo-3D information with better soft-tissue contrast than 2D radiography. DTS images, being reconstructed from limited-angle projections usually spanning 20°–60°, can be acquired in <10 s with imaging dose of <1 cGy, compared to typically 1–2 min and 2–9 cGy for CBCT. These features make DTS a potentially advantageous tool for determining and verifying onboard target positions in radiation therapy. Recent studies have found DTS promising in accurate target verification using either gantry-mounted kV source with kV imager[17–24] or MV source with flat panel detector.[25,26] Applications in brachytherapy were also investigated to be of potential benefit.[27]

However, the applications of the DTS studies listed above are mainly limited to 3D-DTS for static targets verification. For moving targets verification, its localization accuracy can be compromised by target motion. Recently, we developed a 4D-DTS technique to track target motion.[28–31] Through optimizing image acquisition parameters and sorting onboard projections retrospectively, DTS images at different respiration phases could be reconstructed to determine target motion accurately. However, though taking less scan time and dose compared to 4D-CBCT,[32,33] 4D-DTS still requires relatively long scan time [at least a few respiratory cycles (RC)] and higher imaging dose than 3D-DTS, making it less feasible currently.

In this study, we developed a respiration-phase-matched (later referred as "phase-matched") DTS technique which achieves registration accuracy approaching that of 4D-DTS for moving target, but requiring only the same scan time and dose as 3D-DTS. In this technique, we match the motion information between reference DTS (R-DTS) and onboard DTS (OB-DTS) images to improve DTS localization accuracy of moving targets. Because this technique enables fast and accurate moving target localization, it may be suitable for real-time, quasi-instantaneous (within a sub-breathing cycle) moving target verification during radiation therapy, particularly for VMAT. While the techniques of image-matching based on respiration-phase and 3D/4D-DTS have been previously described, our approach provides improved accuracy over nonphase-matched 3D-DTS. Relative to 4D-DTS, our current technique approaches its accuracy, but reduces the imaging dose and acquisition time. Thus, we believe this investigation proposes an incrementally novel concept.

To evaluate the efficacy of this technique, we performed simulation studies using the 4D digital extended cardiac-torso (XCAT) phantom,[34] and measurements with the CIRS 008A dynamic thoracic phantom (Computerized Imaging Reference Systems, Norfolk, VA). In both studies, the efficacy of phase-matched DTS technique for moving targets verification, relative to that of current available 3D-DTS technique, was evaluated for various combinations of respiratory cycle, scan angle, and the fraction of respiratory cycle contained therein. In addition, for phase-matched DTS, the target size, target location, or respiration pattern inconsistencies were investigated for their effects on its verification efficacy.

II. MATERIALS AND METHODS

II.A. Respiration-phase-matched DTS technique

The OB-DTS, reconstructed from limited-angle projections acquired using kV imager, is used to reflect the target's onboard position. Due to the inherent inhomogeneous resolution feature of DTS, registering OB-DTS directly (especially automatically without manual adjustment) to reference CT for setup correction will be error prone.[18,21] So the preferred method in the application of DTS for target verification is to register OB-DTS to a R-DTS reconstructed from reference CT-projected DRRs matching onboard projections' projecting angles. The resulting inherent inhomogeneous resolution feature of R-DTS makes it comparable to OB-DTS for target verification purpose.

For a static target, the only candidate for reference CT is the static 3D reference CT acquired. For a moving target due to respiration, the potential reference CT sets include free-breathing-CT (FB-CT), average intensity projection (AIP) of 4D-CT, maximum intensity projection (MIP) of 4D-CT, minimum intensity projection (MinIP) of 4D-CT, or ten-phase 4D-CT itself.

Currently developed 3D-DTS techniques can only use 3D reference CT. As the position distribution function of target in MIP or MinIP is deviated from the truth, and previous practices typically register the target in AIP or FB-CT with that in onboard CBCT for moving target verification,[7,8,35] we choose AIP and FB-CT as the 3D reference CTs for the 3D-DTS method.

As an improvement to current techniques, we propose here a phase-matched DTS technique that uses the ten-phase 4D-CT dataset directly as the reference CT, shown in Fig. 1.

As illustrated in Fig. 1, the 4D-CT dataset is used as the reference CT to generate DRRs that are matched with corresponding onboard projections. Besides the common projecting angle matching, the phase of each DRR is also matched to that of the corresponding onboard projection.

Figure 2 depicts the phase-matching process in more detail. The OB-DTS is reconstructed using limited-angle onboard kV projections (indicated by the dashed line) acquired when the gantry rotates [Fig. 2(A) and 2(B)]. The respiratory phase of each projection is identified to generate a corresponding DRR using selected 3D CT volume of the same phase (indicated by the bar each dashed line connects) from the 4D-CT dataset [Fig. 2(A)]. The DRRs, "phase-matched" with the corresponding onboard kV projections, are then used to reconstruct a phase-matched R-DTS for comparison with the OB-DTS [Fig. 2(C)].

The efficacy of the phase-matched DTS technique is evaluated through XCAT simulation and CIRS phantom study and compared with that of the 3D-DTS technique. The evaluation

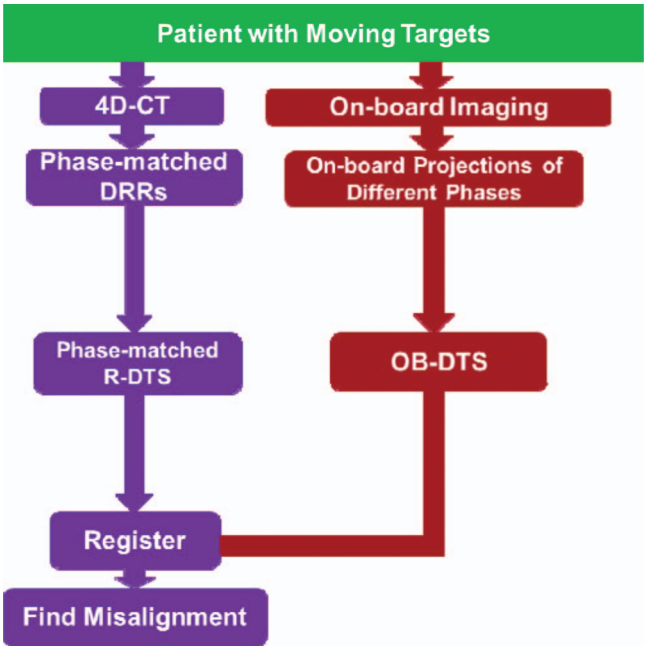

FIG. 1. The phase-matched DTS technique scheme.

and comparison is performed under various combinations of DTS imaging parameters: the RC length, DTS scan angle (β), and respiratory cycle fraction (FX) contained therein. The relation of these parameters, together with the gantry rotation speed (GRS), can be written as

$$\beta = \mathrm{FX} \times \mathrm{RC} \times \mathrm{GRS}. \quad (1)$$

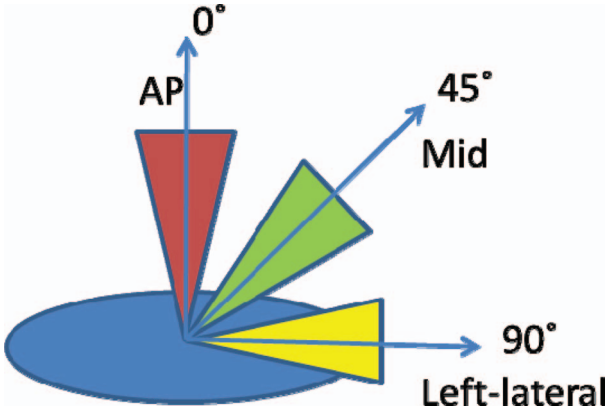

FIG. 3. Three scan directions for DTS reconstruction.

To include the potential variations caused by different scan directions, we evaluated DTS sets with three scan angles: anterior-posterior (AP) (0°), left-lateral (90°), and midway (halfway between AP and left-lateral, 45°), as shown in Fig. 3.

II.B. XCAT simulation

II.B.1. Simulation of reference and onboard images using the 4D XCAT

We used the 4D XCAT, a digital anthropomorphic phantom that can be utilized to produce 4D images according to specified anatomy parameters and respiratory profiles,[34] to generate reference and onboard images. A spherical lesion was

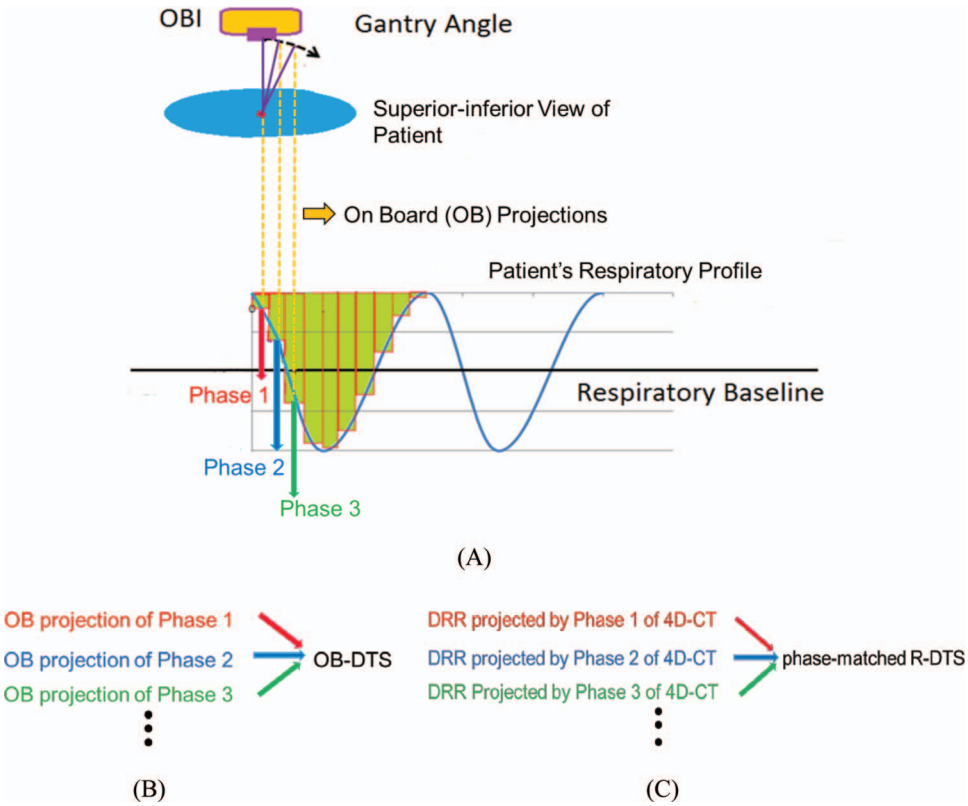

FIG. 2. Scheme illustrating the proposed phase-matched method.

inserted into the lung as the treatment target, and the following image datasets were generated using an inhouse developed GUI interface:

1. Ten-phase 4D-CT dataset, with end expiration at phase 0%, and end inspiration at 40%,
2. AIP from the 4D-CT dataset by averaging each pixel's intensity of the ten phases,
3. FB-CT using mixed-phase slices, with each slice's phase determined by predefined CT imaging speed and rows of detector.

Each phase of 4D-CT, and each 3D-CT, was composed of 126 slices (2.5 mm thick) of 512 × 512 pixels (1 × 1 mm).

Onboard kV projections were simulated using the CT_proj, a subsidiary simulation tool of XCAT. They were generated in full-fan mode at frame rate of ten frames per second (fps) and 6°/s GRS to simulate clinical onboard projection acquisition. Each onboard projection contained 512 × 384 pixels measuring 0.78 × 0.78 mm. The simulated x-ray source was 140 kVp, with 0.05 mAs per projection.

For the simulated onboard kV projections, their phases were accurately calculated using the simulation frame rate, GRS, and respiratory profiles input. One point worth mentioning here is that the onboard projections were generated without the ten-phase approximation—they were generated exactly according to their tags on the respiratory profile trajectory. The phase-determination here only aims to correlate each projection with the reference ten-phase 4D-CT for phase-matching purpose.

II.B.2. Generating DRRs from reference CT

DRRs were generated from reference CT using an inhouse developed ray-tracing technique.[36] Phase-matched DRRs were generated from different reference 4D-CT phases corresponding with onboard projection's phases, while nonphase-matched DRRs were generated from reference AIP/FB-CT with only projecting angles matched.

II.B.3. DTS reconstruction

For reconstruction of DTS images from the onboard projections and DRRs, we used filtered backprojection with Feldkamp–Davis–Kress (FDK) (Ref. 37) algorithm. Each reconstructed DTS dataset contained 512 slices (0.5 mm thick), each with 512 × 320 pixels (0.5 × 0.5 mm). Phase-matched R-DTS$_{4D\text{-}CT}$ was reconstructed from phase-matched DRRs, and 3D R-DTS$_{AIP}$ and R-DTS$_{FB\text{-}CT}$ from nonphase-matched DRRs.

II.B.4. Incorporation of intentional misalignment

The R-DTS and OB-DTS, as both originating from the XCAT, were perfectly aligned. To simulate onboard target position deviation, we introduced intentional misalignment to the R-DTS sets (through misaligning the reference CT sets), using inhouse developed software to shift them in three directions, singly or in combination: (shift, 0, 0), (0, shift, 0), (0, 0, shift), and (shift, shift, shift). Three shift values: 2, 5, and 10 mm were used. So for each reference CT set, there were 4 × 3 = 12 misalignment scenarios in total.

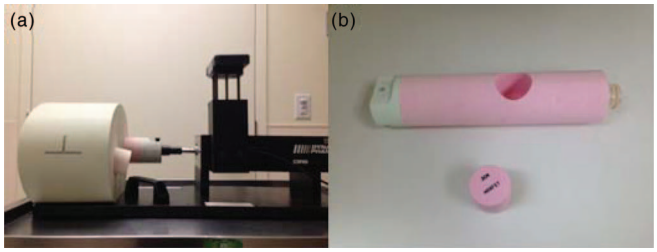

FIG. 4. (a) and (b) The CIRS 008A dynamic thoracic phantom.

II.B.5. Scenarios tested

Different simulation scenarios were investigated by altering the acquisition parameters, the respiratory profiles as well as the size and location of the spherical targets inserted. In this simulation study, for spherical target of 30 mm diameter in the middle of lung, three different FX values: 2/3, 1, and 4/3; and three β values: 20°, 30°, and 40° were tested. In total, nine different combinations of β, FX, and RC were investigated (Table I). In addition, 30 mm spherical targets near three other locations: 1. chest wall, 2. diaphragm, 3. mediastinum were tested for fixed $\beta = 30°$ and three FXs: 2/3, 1, and 4/3. 15 mm spherical targets near the same three locations with fixed $\beta = 30°$ and FX = 4/3 were also investigated.

II.C. Motion phantom measurement study

We performed measurements using the CIRS 008A dynamic thoracic phantom [Fig. 4(a)] to further assess the efficacy of our method. A 30 mm diameter insert [Fig. 4(b)] of uniform density was placed in the lung-equivalent rod of the phantom to mimic the target. The insert moves according to user-specified respiratory profiles using the CIRS Motion Control software. A GE lightspeed RT scanner (GE Healthcare, Waukesha, WI) was used to acquire 3D CT of the static phantom, and ten-phase reference 4D-CT and FB-CT of the moving phantom. The AIP was then generated from the 4D-CT using the same method described in Sec. II.B.1.

Onboard kV projection acquisition was performed using a Truebeam LINAC (Varian Medical Systems, Palo Alto, CA). To align the images from the GE CT to the Truebeam kV, a CBCT of the static phantom was acquired and registered to the 3D CT from the GE CT for initial setup correction. After initial setup correction, for onboard kV projection acquisitions of each respiratory profile, intentional

TABLE I. Different β, FX, and RC combinations tested for spherical target of 30 mm diameter in the middle of lung.

RC(s)	$\beta = 20°$	$\beta = 30°$	$\beta = 40°$
FX = 2/3	5	7.5	10
FX = 1	3.3	5	6.7
FX = 4/3	2.5	3.8	5

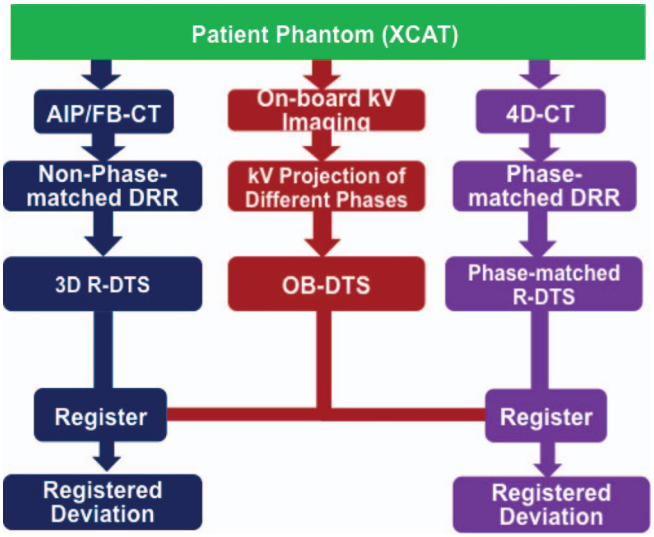

FIG. 5. The general scheme of simulation/measurement study.

misalignment of (0, 0, 10 mm), (0, 10 mm, 0), (10 mm, 0, 0), and (5, 5, 5 mm) were applied to the couch to simulate patient setup errors. The onboard projections were acquired at GRS $\approx 6^\circ$/s with ~11 fps frame rate in full-fan mode. Each projection was downsampled to 512 × 384 pixels, with each pixel 0.78 × 0.78 mm in dimension. The energy of the kV source was 100 kVp, with 0.4 mAs per projection.

The phase of each onboard projection was determined through manually checking the images to identify projections with the target's trajectory peaks/valleys. For the two projections of adjoining respiration peaks/valleys, the phases of projections in between are automatically assigned through dividing these projections into ten equal bins. Similar to XCAT simulation, different β, FX, and RC combinations were tested. The respiratory profile (frequency and amplitude) inconsistencies from R-DTS to OB-DTS were also studied for the potential influences on target verification accuracy.

II.D. Registration method

The intentionally misaligned R-DTS and OB-DTS images were spatially registered using inhouse developed automatic registration software.[21] The similarity metric used in the automatic registration was mutual information (MI),[38] and the optimization was based on downhill simplex algorithm.[39] Internal target volume (ITV) with a 5 mm margin was selected as the region of interest (ROI) for registration. Note that the registration method registered both rotations and shifts, although the intentional misalignment was shifts only.

II.E. Evaluation method

We registered the OB-DTS to R-DTS (R-DTS$_{4D\text{-}CT}$, R-DTS$_{AIP}$, and R-DTS$_{FB\text{-}CT}$), which were all subjected to the known intentional misalignment (see Secs. II.B.4 and II.C). The registration errors were used as the criterion to evaluate the efficacy of both phase-matched and 3D-DTS methods (Fig. 5).

In detail, the 3D shift vector registration error was used as a quantitative value to measure the registration accuracy. In addition, a "2 mm and 1°" passing criterion was also defined to qualify the registration accuracy. "2 mm" denotes the 3D shift vector registration error should be smaller or equal to 2 mm and "1°" indicates any rotational registration error around axis x, y, or z should be smaller or equal to 1°. Only registrations meeting the two criteria concurrently were regarded as "passing."

III. RESULTS

III.A. XCAT simulation

Figure 6(A) shows XCAT-simulated OB-DTS in the AP scan direction for 30 mm target in the middle of lung (RC = 5 s, FX = 1, and $\beta = 30^\circ$). The other panels, generated with the same parameters are: R-DTS$_{4D\text{-}CT}$ [panel (B)], R-DTS$_{AIP}$ [panel (C)], and R-DTS$_{FB\text{-}CT}$ [panel (D)]. No misalignment was applied. The MI indices calculated between OB-DTS and each R-DTS are indicated in panels (B)–(D), and evince that the R-DTS$_{4D\text{-}CT}$ is best matched to the OB-DTS.

Figure 7 shows boxplots of 3D shift vector registration errors between XCAT-simulated OB-DTS and the different R-DTS sets for β values of 20° [panel (A)], 30° [panel (B)], and 40° [panel (C)], of a 30 mm target in the middle of lung. In each panel, subpanels are for variable FX values of 2/3, 1, and 4/3, respectively. Each boxplot includes 36 points [12 misalignment scenarios (see Sec. II.B.4) × 3 scan directions (Fig. 3)]. It is clearly evident that the phase-matched technique, i.e., using R-DTS$_{4D\text{-}CT}$, is the most accurate, for all combinations of β and FX values. Comparing R-DTS$_{AIP}$ with R-DTS$_{FB\text{-}CT}$, the former provides more accurate registration results. And the results of R-DTS$_{AIP}$ are better for FX = 1 than for FX = 2/3. For the 324 different scenarios simulated, the respiration-phase-matched DTS technique localizes the 3D target position to errors of 1.07 ± 0.57 mm (mean ± S.D.), as compared to (a) 2.58 ± 1.37 and (b) 7.37 ± 4.18 mm, for 3D-DTS using 3D reference CT of (a) AIP and (b) FBCT.

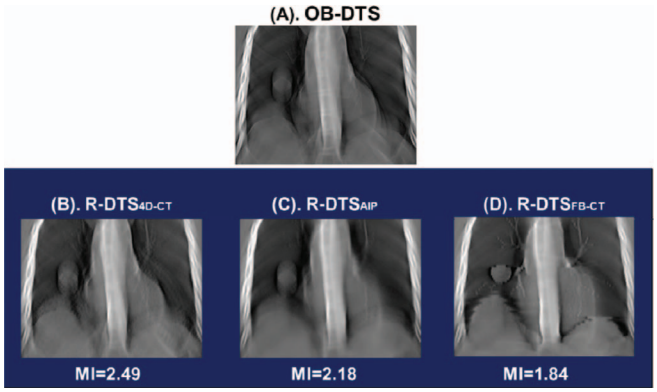

FIG. 6. Figures of 30° OB-DTS [panel (A)] and corresponding R-DTS$_{4D\text{-}CT}$ [panel (B)], R-DTS$_{AIP}$ [panel (C)], and R-DTS$_{FB\text{-}CT}$ [panel (D)] with AP scan direction for 30 mm target in the middle of lung, with RC = 5 s and FX = 1.

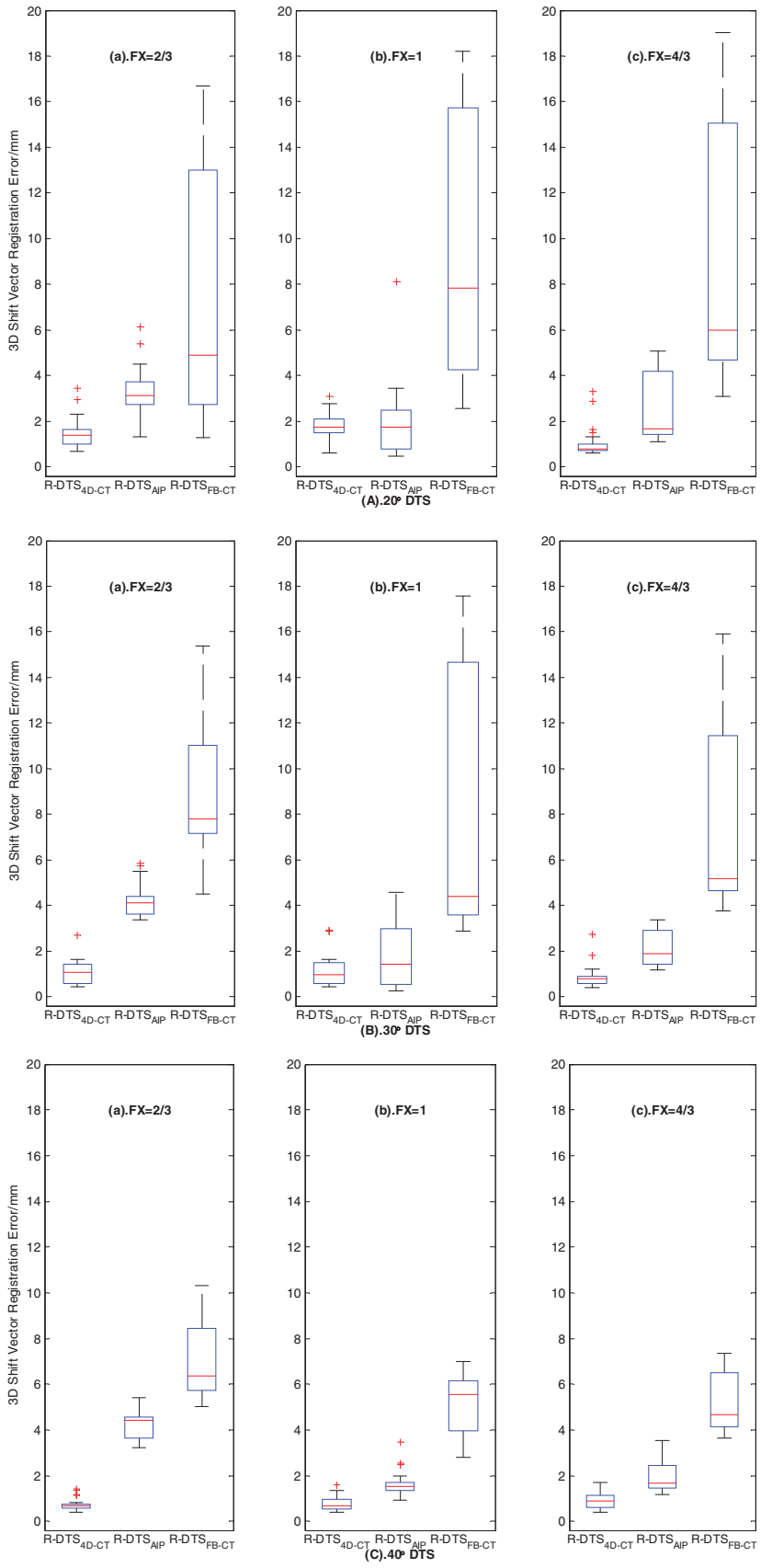

FIG. 7. Boxplots of 3D shift vector registration error between OB-DTS and R-DTS sets of scan angles: 20° [panel (A)], 30° [panel (B)], and 40° [panel (C)], for cases with a 30 mm target in the middle of lung. In each panel, subpanels (a)–(c) are for variable FX values of 2/3, 1, and 4/3, respectively. For each box, the upper edge, central line, and lower edge represent the 75 percentile ($Q3$), median, and 25 percentile ($Q1$) of the data, respectively. The lower error bar extends to the value equal to $Q1 - 1.5 \times (Q3 - Q1)$, and the upper error bar extends to $Q1 + 1.5 \times (Q3 - Q1)$. The "+" in the plots are outliers outside of the error bars.

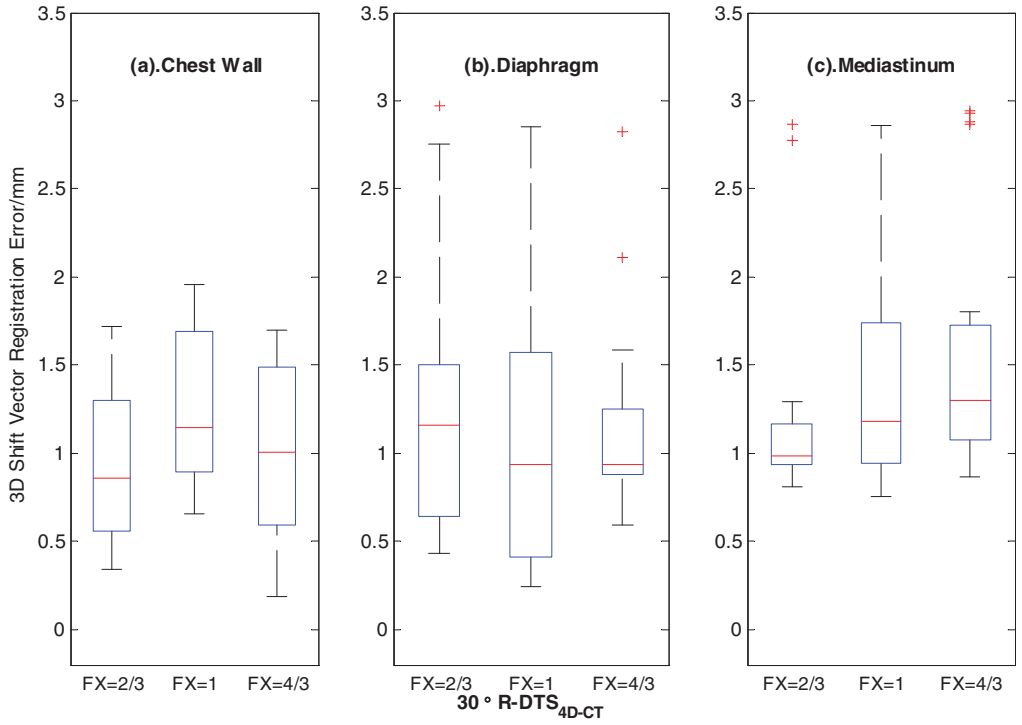

FIG. 8. Boxplots of 3D shift vector registration error between 30° OB-DTS and R-DTS$_{4D\text{-}CT}$ for a 30 mm target near three different locations: chest wall [subpanel (a)], diaphragm [subpanel (b)], and mediastinum [subpanel (c)] for FX = 2/3, 1, and 4/3.

The following results focus on the robustness of using the phase-matched method to determine the position of XCAT-simulated targets of various sizes and locations.

Figure 8 shows the boxplots of 3D shift vector registration errors between XCAT-simulated OB-DTS and R-DTS$_{4D\text{-}CT}$ of $\beta = 30^\circ$ for a 30 mm target near three different locations: chest wall [subpanel (a)], diaphragm [subpanel (b)], and mediastinum [subpanel (c)].

Figure 9 shows the registration results for XCAT-simulated 15 mm target near three different locations described above.

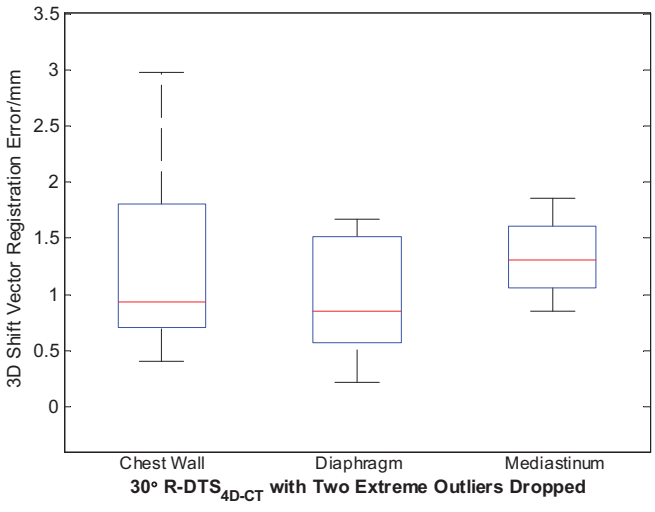

FIG. 9. Boxplots of 3D shift vector registration error between 30° OB-DTS and R-DTS$_{4D\text{-}CT}$ for a 15 mm target near three different locations: chest wall, diaphragm, and mediastinum for FX = 4/3.

In Fig. 9, two extreme outliers of large 3D shift vector registration errors are excluded from the boxplot, of which the applied intentional misalignment is (10, 10, 10 mm) for both. Compared with the other registration results, the two extreme outliers (one for target near diaphragm and the other for target near mediastinum) have much larger 3D shift vector registration errors: 49.28 mm for the former one and 29.97 mm for the latter.

Table II summarizes the registration passing rates with regard to the "2 mm and 1°" passing criterion for all the XCAT-simulated scenarios described in Sec. II.B.5. The passing rates are consistent with what are shown in Figs. 7–9.

III.B. CIRS phantom study

Figure 10(A) shows the registration results of CIRS phantom study for fixed RC = 5 s and variable FXs: 2/3, 1, and 4/3. The corresponding βs are 20°, 30°, and 40°, respectively. The phase-matched R-DTS$_{4D\text{-}CT}$ provides the most accurate target position localization among all.

Figure 10(B) shows the registration results of CIRS phantom study for fixed $\beta = 30^\circ$ and variable FXs: 2/3, 1, and 4/3. The corresponding RCs are 7.5, 5, and 3.8 s, respectively. The target localization results of phase-matched R-DTS$_{4D\text{-}CT}$ are also better than R-DTS$_{AIP}$ and R-DTS$_{FB\text{-}CT}$.

For the 60 scenarios evaluated, the respiration-phase-matched DTS technique localizes the 3D target position to errors of 1.24 ± 0.87 mm, as compared to (a) 2.42 ± 1.80 and (b) 5.77 ± 6.45 mm, for 3D-DTS using 3D reference CT of (a) AIP and (b) FBCT. Table III summarizes the corresponding registration passing rates according to the "2 mm

TABLE II. Passing rates of all XCAT-simulated scenarios according to the "2 mm and 1°" passing criterion.

(A) Comparison between phase-matched and 3D-DTS techniques

			R-DTS$_{4D\text{-}CT}$	R-DTS$_{AIP}$	R-DTS$_{FB\text{-}CT}$
		FX		20° β	
		2/3	**86%**	**3%**	**3%**
		1	**72%**	**69%**	**0%**
		4/3	**94%**	**50%**	**0%**
				30° β	
XCAT phantom study A	30 mm target in the middle of lung	2/3	**94%**	**0%**	**0%**
		1	**94%**	**56%**	**0%**
		4/3	**97%**	**58%**	**0%**
				40° β	
		2/3	**100%**	**0%**	**0%**
		1	**94%**	**28%**	**0%**
		4/3	**100%**	**31%**	**0%**

(B) Robustness test of phase-matched DTS technique for different target size/location combinations

	R-DTS$_{4D\text{-}CT}$	FX	30° β
XCAT phantom study B	30 mm target near chest wall	2/3	**100%**
		1	**97%**
		4/3	**100%**
	30 mm target near diaphragm	2/3	**89%**
		1	**94%**
		4/3	**94%**
	30 mm target near mediastinum	2/3	**86%**
		1	**83%**
		4/3	**92%**
	15 mm target near chest wall	4/3	**78%**
	15 mm target near diaphragm	4/3	**64%**
	15 mm target near mediastinum	4/3	**69%**

and 1°" passing criterion for CIRS phantom study described above. The passing rates of phase-matched R-DTS$_{4D\text{-}CT}$ are the highest among all, consistent with what are shown in Fig. 10.

Figures 11 and 12 show the registration results of CIRS phantom study for 30° DTS with varying RC and respiratory amplitude introduced as respiration inconsistencies between R-DTS and OB-DTS. In Fig. 11, it can be observed that the variations of RC has less impact on the registration accuracy of the phase-matched DTS technique. R-DTS$_{4D\text{-}CT}$ still has the best registration accuracy among all. In Fig. 12, it can be observed that the variations of amplitude, on the other hand, lead to less accurate registration results, especially when amplitude changes from 10 to 20 mm.

TABLE III. Passing rates of CIRS phantom study in Fig. 10 according to the "2 mm and 1°" passing criterion.

		R-DTS$_{4D\text{-}CT}$	R-DTS$_{AIP}$	R-DTS$_{FB\text{-}CT}$
	FX		5 s RC	
	2/3	**67%**	**17%**	**17%**
30 mm target in the CIRS phantom	1	**92%**	**67%**	**17%**
	4/3	**100%**	**83%**	**8%**
	FX		30° β	
	2/3	**83%**	**42%**	**25%**
	1	**92%**	**67%**	**17%**
	4/3	**92%**	**75%**	**75%**

IV. DISCUSSION

IV.A. Phase-matched vs 3D-DTS technique

The results of both the XCAT simulation [Fig. 7, Table II(A)] and the CIRS phantom studies (Fig. 10, Table III) clearly show that the use of phase-matched R-DTS$_{4D\text{-}CT}$ yields improved registration accuracy, as compared to that using 3D R-DTS$_{AIP}$ and R-DTS$_{FB\text{-}CT}$. Comparing R-DTS$_{FB\text{-}CT}$ and R-DTS$_{AIP}$, the former provides worse registration accuracy [Figs. 7 and 10, Tables II(A) and III]. This is because, unlike AIP which is a volume of averaged phases, FB-CT is a volume of mixed phases such that the target location and shape can be greatly shifted and distorted. So R-DTS$_{FB\text{-}CT}$ reconstructed from FB-CT will lead to poor target registration.

The registration results using R-DTS$_{4D\text{-}CT}$, for a given β, is insensitive to the values of FX and RC [Figs. 7 and 10(B), Tables II(A) and III]. In contrast, changes in FX or RC affect the registration accuracy with the use of R-DTS$_{AIP}$ [Figs. 7 and 10(B), Tables II(A) and III]. This is due to the

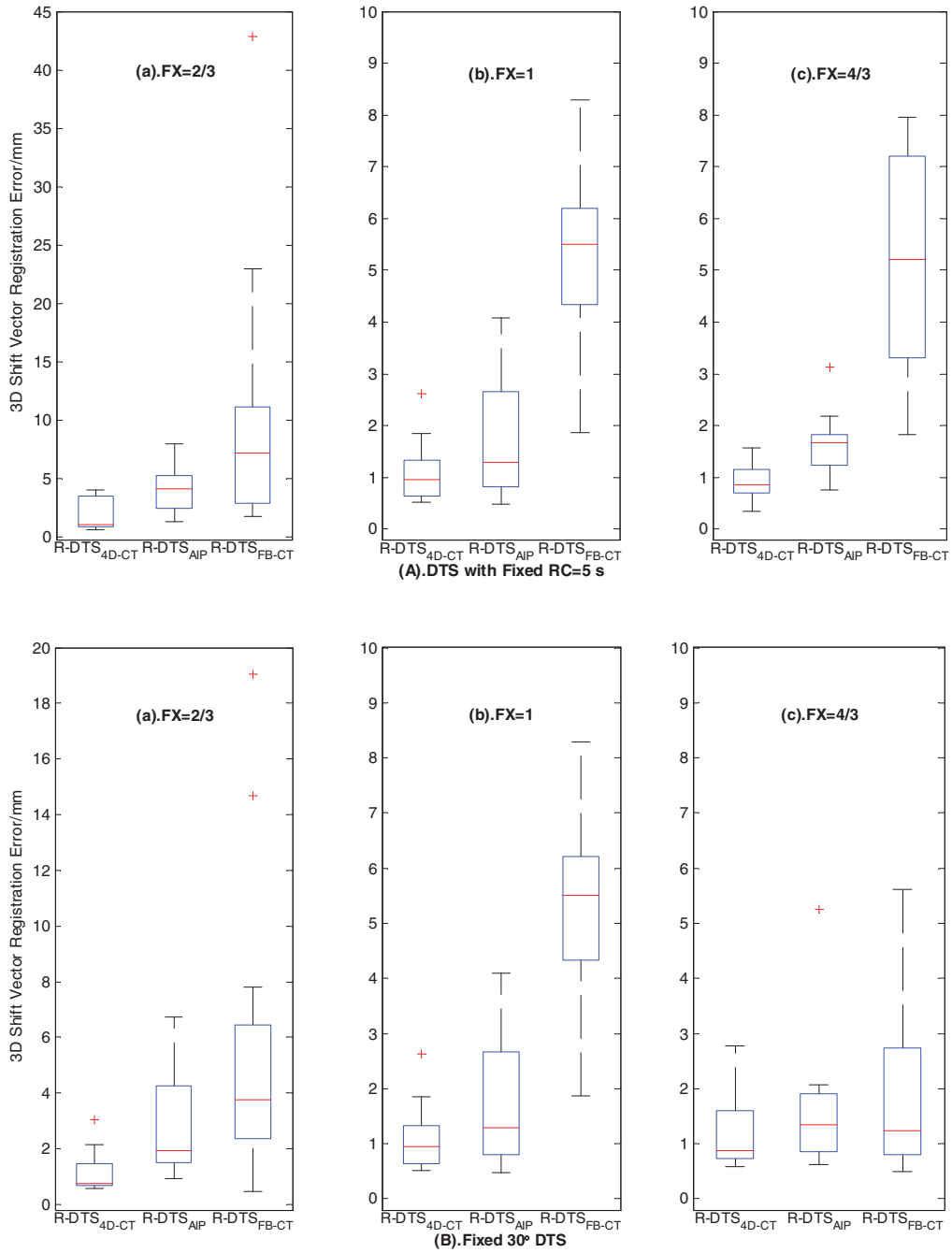

FIG. 10. Boxplots of 3D shift vector registration error between OB-DTS and R-DTS sets of fixed RC = 5s [panel (A)] and fixed $\beta = 30^\circ$ [panel (B)], for the CIRS phantom study. In each panel, subpanels (a)–(c) are for variable FX values of 2/3, 1, and 4/3, respectively.

generation mechanism of AIP, which is built by averaging all the ten phases of 4D-CT. For FX < 1, OB-DTS only covers part of the motion trajectory (<10 phases) while R-DTS$_{AIP}$ covers entire target trajectory (all ten phases) as it is generated from AIP. The ITV shapes in OB-DTS and R-DTS$_{AIP}$ are different and registering them together will lead to errors. Conversely, when FX is larger than 1, registration inaccuracy may also arise because of unequal weightings of different phases in OB-DTS [Fig. 7(A), Table II(A)] compared with equal weightings of those in R-DTS$_{AIP}$.

When FX or RC is fixed, the registration results of R-DTS$_{4D\text{-}CT}$ generally improve when scan angle β increases [Figs. 7 and 10(A); Tables II(A) and III], as larger scan angle provides more information for accurate registration.

IV.B. Robustness of phase-matched DTS technique for target size/location variations

For the larger (30 mm) target, the accuracy of target registration for phase-matched DTS technique is slightly location-dependent [Fig. 8, Table II(B)], with worst result observed for target near the mediastinum, probably due to the interferences from the surrounding simulated soft tissues. The registration accuracy for the smaller (15 mm) target is worse

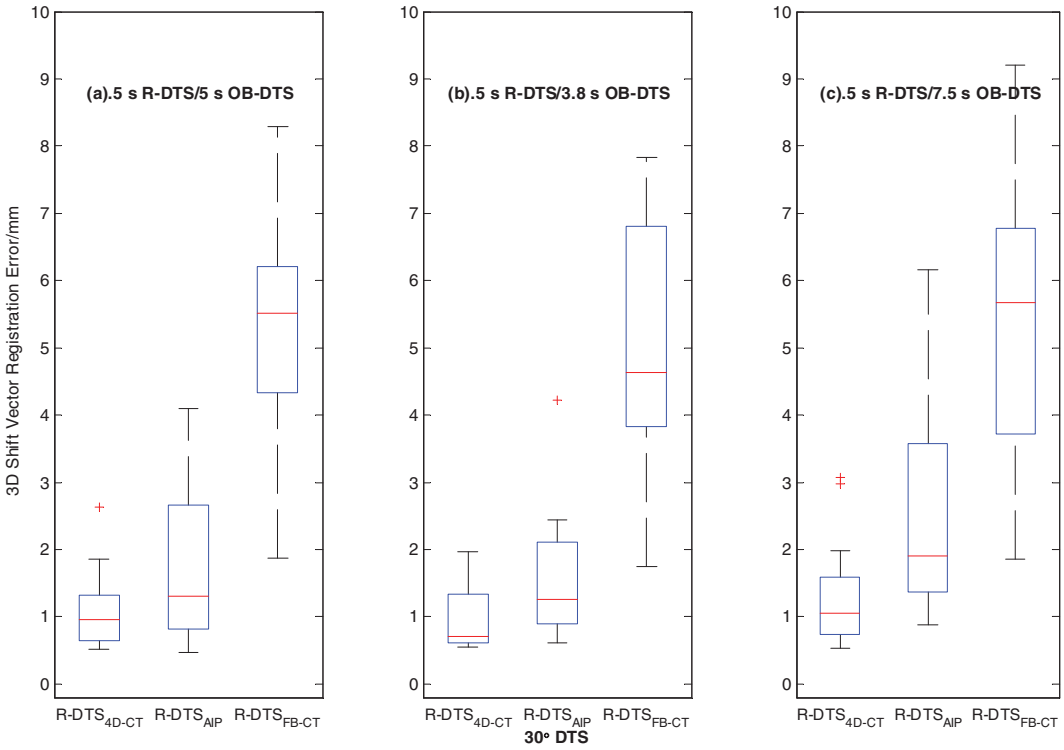

FIG. 11. Boxplots of 3D shift vector registration error between OB-DTS and R-DTS sets, of fixed $\beta = 30^\circ$ for the CIRS phantom study. The respiratory cycle of R-DTS sets is fixed at 5 s. The respiratory cycles of corresponding OB-DTS sets are: 5 s [subpanel (a)], 3.8 s [subpanel (b)], and 7.5 s [subpanel (c)], respectively.

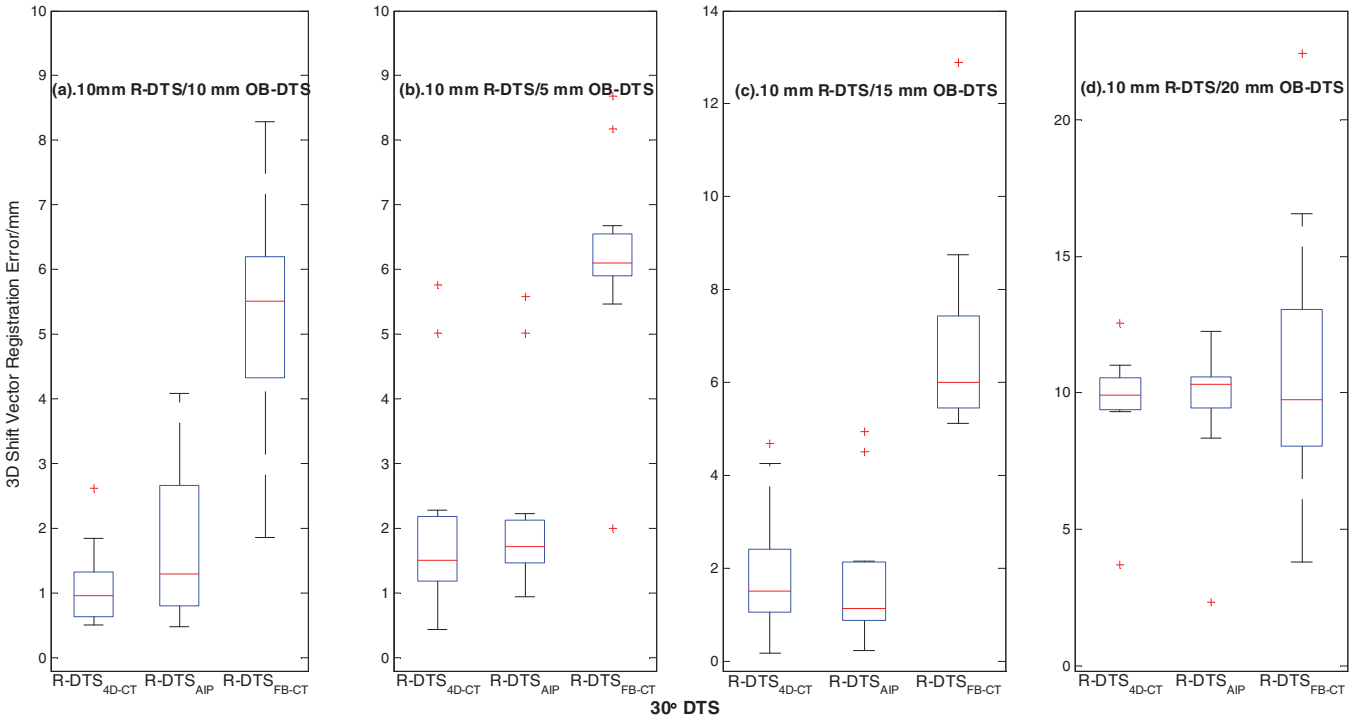

FIG. 12. Boxplots of 3D shift vector registration error between OB-DTS and R-DTS sets, of fixed $\beta = 30^\circ$ and FX = 1 for the CIRS phantom study. The respiratory amplitude of R-DTS sets is fixed at 10 mm. The respiratory amplitudes of corresponding OB-DTS sets are: 10 mm [subpanel (a)], 5 mm [subpanel (b)], 15 mm [subpanel (c)], and 20 mm [subpanel (d)], respectively.

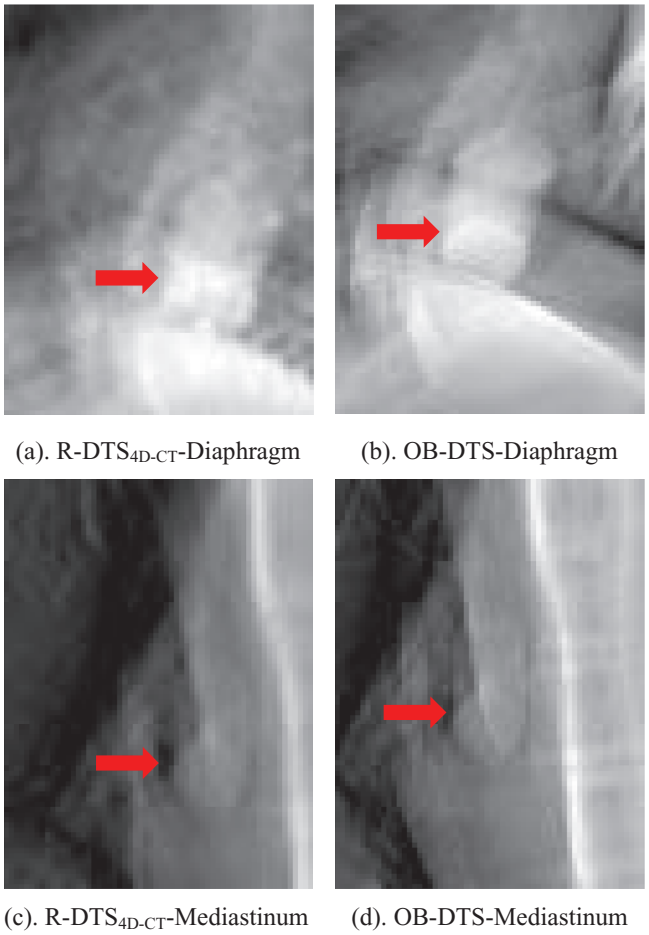

FIG. 13. Comparison between the slices from (a) and (c) R-DTS$_{4D\text{-}CT}$ and (b) and (d) OB-DTS for the two extreme outliers of failed registration (tumor locations indicated by red arrows).

than that for the larger (30 mm) target [Fig. 9, Table II(B)], probably due to less ITV information available, causing mutual information fluctuations and the downhill simplex optimization algorithm to be trapped in local maximums. Nevertheless, the 3D shift vector registration errors are mostly <2 mm except for two extreme outliers: one for a target near diaphragm and the other mediastinum. For the diaphragm case, by changing the initial misalignment guess from (0, 0, 0 mm) to (10, 10, 10 mm) in the registration algorithm, the 3D shift vector registration error of the final registration result declines from 49.28 to 1.49 mm. The corresponding mutual information between the registered OB-DTS and R-DTS$_{4D\text{-}CT}$ increases from 1.40 to 2.15. For the mediastinum case, through the same change of initial misalignment guess, the 3D shift vector registration error declines from 29.97 to 0.91 mm. The corresponding mutual information increases from 1.69 to 2.86. We conjecture that such extreme outliers may be avoided with more robust registration algorithms better at global maximum searching such as simulated annealing.[40] Another solution is to apply manual adjustment after the automatic registration. As shown in Fig. 13, manual adjustment is possible when appropriate window is used.

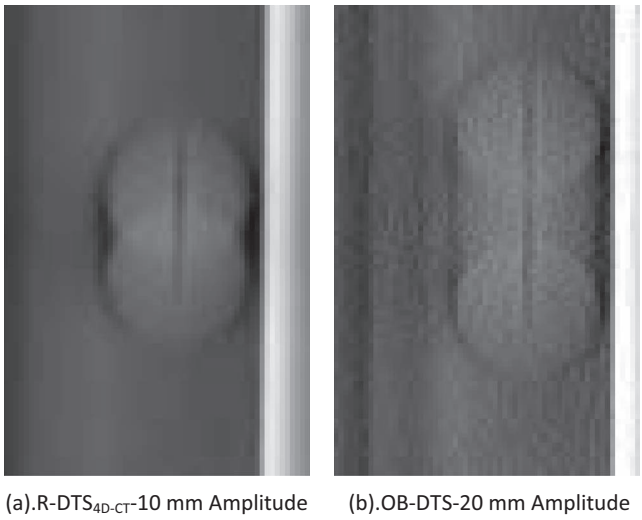

FIG. 14. Comparison between the shapes of ITVs of (a) R-DTS$_{4D\text{-}CT}$ and (b) OB-DTS with 10 mm amplitude variation.

IV.C. Robustness of phase-matched DTS technique for respiration inconsistencies

As presented in Sec. III (Figs. 11 and 12), inconsistencies in RC and respiration amplitude between the R-DTS and OB-DTS affect registration accuracy differently. Specifically, the registration accuracy using phase-matched technique is still the highest, and is insensitive to RC inconsistencies between R-DTS$_{4D\text{-}CT}$ and OB-DTS (Fig. 11). This is understandable as the target positions at the same phase for different RCs are approximately the same, so the blurring target in R-DTS$_{4D\text{-}CT}$ still matches that in OB-DTS. On the other hand, for respiration amplitude inconsistencies, the target positions will be distributed differently in the phase-matched DRRs vis-à-vis the onboard kV projections, leading to registration errors, as observed in Fig. 12. This is further illustrated in Fig. 14: for a 10 mm amplitude variation, the shapes of two ITVs (in R-DTS$_{4D\text{-}CT}$ and OB-DTS) are very different, leading to errors in image registration. Manual adjustment will be needed for this situation.

IV.D. Scan angle β

In terms of the scan angle needed for reliable phase-matched DTS registration, our study results show 30° is desirable [Figs. 7–10, Tables II(A) and III], although 20° may also be acceptable [Fig. 7(A), Table II(A)]. If *a priori* information and different DTS reconstruction method are used, as proposed in our previous study,[41,42] even smaller scan angle, e.g., 10°, may produce accurate results.

IV.E. The phase-identification of onboard kV projections

As mentioned in Secs. II.B.1 and II.C, for the XCAT study, the phases were accurately calculated through the predefined parameters. For the CIRS phantom measurement study, the phase were determined through manually identifying the peak

inspiration/expiration by observing the target's trajectory in onboard projections.

For real clinical application, the manual phase identification method used for the CIRS phantom study is feasible while the interobserver variations and the extra time needed for data processing should be considered. Besides this method, other phase-detection methods based on features exhibited in onboard projections include: the Fourier transform technique utilizing Fourier domain variations between projections,[32] the Amsterdam shroud technique using extracted diaphragm edge displacements or other comparable techniques,[43] the 2D/2D matching technique using DRRs generated from all 4D-CT phases to find the phase best matched with the onboard projection,[44] etc. These methods can provide very accurate phase identification results, but one common deficiency is that their efficacies are usually relying on the visibility of the selected internal markers/features in the projections.

Compared with the above methods using internal features/markers, the methods using external markers such as Varian's Real-time Position Management (RPM) system[45] and the strain-gauged Anzai belt system (Anzai Medical Systems, Tokyo, Japan) (Ref. 46) provide faster and more convenient alternatives for phase tagging. But they suffer from problems of possible unsynchronization and mismatches between external marker motion and the actual internal anatomy motion.[47,48] One possible solution of this issue is to combine external motion tracking with internal motion tracking through correcting the phase shifts in external motion using limited phases identified by internal tracking.

IV.F. The registration technique

In this paper, the simulated onboard misalignment is solved by 3D-3D registration between the reconstructed R-DTS and OB-DTS. Another approach to register the misalignment is to match the DRRs to onboard projections directly without reconstruction, and realign the 4D-CT to maximize the similarities between DRRs and onboard projections. Compared with the 3D-3D registration performed by us, the latter 4D-2D registration is an iterative method that requires more computation power and registration time. Moreover, considering the potential benefit of 3D tomographic registration over 2D planar projection registration, we adopt the 3D R-DTS to 3D OB-DTS registration technique, which is more efficient, more clinically implementable and can achieve sub-mm accuracy.

IV.G. Limitations of the current work

In this preliminary study, simulated onboard misalignment is limited to shift only. Due to the inhomogeneous resolution feature present in DTS, the registration algorithm used in this study will not provide accurate registration for rotational misalignment, especially for out-of-plane rotations.[21] Currently, a more advanced phase-matched DTS registration algorithm is under development based on the hybrid method we developed before to better register rotational misalignment.[21] It will be investigated in future study. For the current study, we use shift-only misalignment to test the feasibility of using the phase-matched DTS for moving target localization.

In this study, the data tested are limited to those generated by XCAT simulation and CIRS phantom study. Use of patient cases for this study is challenging at this time: unlike the XCAT or CIRS phantom in this study, it is hard to obtain a ground truth of patient misalignment to evaluate the registration accuracy of phase-matched DTS. Although 4D-CBCT can be the standard for evaluating target's true misalignment, it is not currently available in the clinic. Evaluation using patient cases will be optimal when this ground truth or its reliable alternative becomes available.

V. CONCLUSIONS

The phase-matched DTS technique generates each DRR for a corresponding onboard kV projection with phase matched between each other and reconstructs phase-matched R-DTS$_{4D\text{-}CT}$ from the DRRs to compare with OB-DTS. The preliminary results showed that this technique substantially improved the accuracy of moving targets localization, as compared to the 3D-DTS technique. The phase-matched DTS technique is also more robust, being minimally affected by variations of respiratory cycle length or fraction of respiration cycle contained within the DTS scan. Increasing scan angle improved the registration accuracy of phase-matched DTS technique. For different target locations, the targets near the chest wall or in the middle of lung provided better registration accuracy compared to those near the mediastinum and diaphragm. Larger targets provided better registration accuracy than small targets. Finally, inconsistencies of respiration cycle length between R-DTS and OB-DTS minimally affected the efficacy of the phase-matched DTS technique, but inconsistencies of respiration amplitude led to larger registration discrepancies.

XCAT simulation and CIRS phantom studies show phase-matched DTS substantially improves the registration accuracy of moving targets compared to traditional 3D-DTS methods. It can potentially become an effective tool for prior-treatment patient setup correction, post-treatment target location verification or real-time, and quasi-instantaneous target tracking during arc delivery. Future evaluation with patient cases is warranted.

ACKNOWLEDGMENTS

This work is partially supported by a research grant from Varian Medical Systems. The authors want to thank Dr. Paul Segars for use of his XCAT program, Dr. Jing Cai for use of his XCAT GUI, and Irina vergalasova for all the profound and intriguing discussions of this project.

[a]Author to whom correspondence should be addressed. Electronic mail: you.zhang@duke.edu; Telephone: (919) 681-9658; Fax: (919) 681-7183.

[1]Intensity Modulated Radiation Therapy Collaborative Working Group, "Intensity-modulated radiotherapy: Current status and issues of interest," Int. J. Radiat. Oncol., Biol., Phys. **51**(4), 880–914 (2001).

[2]K. Otto, "Volumetric modulated arc therapy: IMRT in a single gantry arc," Med. Phys. **35**(1), 310–317 (2008).
[3]L. Xing *et al.*, "Overview of image-guided radiation therapy," Med. Dosim. **31**(2), 91–112 (2006).
[4]T. S. Hong *et al.*, "The impact of daily setup variations on head-and-neck intensity-modulated radiation therapy," Int. J. Radiat. Oncol., Biol., Phys. **61**(3), 779–788 (2005).
[5]D. A. Jaffray *et al.*, "Flat-panel cone-beam computed tomography for image-guided radiation therapy," Int. J. Radiat. Oncol., Biol., Phys. **53**(5), 1337–1349 (2002).
[6]T. G. Purdie *et al.*, "Cone-beam computed tomography for on-line image guidance of lung stereotactic radiotherapy: Localization, verification, and intrafraction tumor position," Int. J. Radiat. Oncol., Biol., Phys. **68**(1), 243–252 (2007).
[7]A. R. Yeung *et al.*, "Tumor localization using cone-beam CT reduces setup margins in conventionally fractionated radiotherapy for lung tumors," Int. J. Radiat. Oncol., Biol., Phys. **74**(4), 1100–1107 (2009).
[8]I. S. Grills *et al.*, "Image-guided radiotherapy via daily online cone-beam CT substantially reduces margin requirements for stereotactic lung radiotherapy," Int. J. Radiat. Oncol., Biol. Phys. **70**(4), 1045–1056 (2008).
[9]F. F. Yin *et al.*, "Integration of cone-beam CT in stereotactic body radiation therapy," Technol. Cancer Res. Treat. **7**(2), 133–139 (2008).
[10]W. Y. Song *et al.*, "A dose comparison study between XVI and OBI CBCT systems," Med. Phys. **35**(2), 480–486 (2008).
[11]T. R. Willoughby *et al.*, "Target localization and real-time tracking using the Calypso 4D localization system in patients with localized prostate cancer," Int. J. Radiat. Oncol., Biol., Phys. **65**(2), 528–534 (2006).
[12]X. Zhu *et al.*, "Tradeoffs of integrating real-time tracking into IGRT for prostate cancer treatment," Phys. Med. Biol. **54**(17), N393–N401 (2009).
[13]J. T. Dobbins III and D. J. Godfrey, "Digital x-ray tomosynthesis: Current state of the art and clinical potential," Phys. Med. Biol. **48**(19), R65–R106 (2003).
[14]T. D. James *et al.*, "Digital tomosynthesis of the chest for lung nodule detection: Interim sensitivity results from an ongoing NIH-sponsored trial," Med. Phys. **35**(6), 2554–2557 (2008).
[15]T. Gomi, "X-ray digital linear tomosynthesis imaging for artificial pulmonary nodule detection," J. Clin. Imaging Sci. **1**, 16 (2011).
[16]T. Gomi *et al.*, "Comparison between chest digital tomosynthesis and CT as a screening method to detect artificial pulmonary nodules: A phantom study," Br. J. Radiol. **85**(1017), e622–e629 (2012).
[17]D. J. Godfrey *et al.*, "Digital tomosynthesis with an on-board kilovoltage imaging device," Int. J. Radiat. Oncol., Biol., Phys. **65**(1), 8–15 (2006).
[18]D. J. Godfrey *et al.*, "Evaluation of three types of reference image data for external beam radiotherapy target localization using digital tomosynthesis (DTS)," Med. Phys. **34**(8), 3374–3384 (2007).
[19]Q. J. Wu *et al.*, "On-board patient positioning for head-and-neck IMRT: Comparing digital tomosynthesis to kilovoltage radiography and cone-beam computed tomography," Int. J. Radiat. Oncol., Biol., Phys. **69**(2), 598–606 (2007).
[20]S. Yoo *et al.*, "Clinical evaluation of positioning verification using digital tomosynthesis and bony anatomy and soft tissues for prostate image-guided radiotherapy," Int. J. Radiat. Oncol., Biol., Phys. **73**(1), 296–305 (2009).
[21]L. Ren *et al.*, "Automatic registration between reference and on-board digital tomosynthesis images for positioning verification," Med. Phys. **35**(2), 664–672 (2008).
[22]J. S. Maltz *et al.*, "Fixed gantry tomosynthesis system for radiation therapy image guidance based on a multiple source x-ray tube with carbon nanotube cathodes," Med. Phys. **36**(5), 1624–1636 (2009).
[23]G. Pang and J. A. Rowlands, "Just-in-time tomography (JiTT): A new concept for image-guided radiation therapy," Phys. Med. Biol. **50**(21), N323–N330 (2005).
[24]A. Mestrovic *et al.*, "Integration of on-line imaging, plan adaptation and radiation delivery: Proof of concept using digital tomosynthesis," Phys. Med. Biol. **54**(12), 3803–3819 (2009).
[25]M. Descovich *et al.*, "Characteristics of megavoltage cone-beam digital tomosynthesis," Med. Phys. **35**(4), 1310–1316 (2008).
[26]G. Pang *et al.*, "Megavoltage cone beam digital tomosynthesis (MV-CBDT) for image-guided radiotherapy: A clinical investigational system," Phys. Med. Biol. **53**(4), 999–1013 (2008).
[27]J. Lee, X. Liu, A. K. Jain, J. L. Prince, and G. Fichtinger, "Tomosynthesis-based radioactive seed localization in prostate brachytherapy using modified distance map images," Proc. IEEE Int. Symp. Biomed. Imaging, 680–683 (2008).
[28]J. Maurer *et al.*, "On-board four-dimensional digital tomosynthesis: First experimental results," Med. Phys. **35**(8), 3574–3583 (2008).
[29]J. Maurer, T. Pan, and F. F. Yin, "Slow gantry rotation acquisition technique for on-board four-dimensional digital tomosynthesis," Med. Phys. **37**(2), 921–933 (2010).
[30]J. Santoro *et al.*, "Evaluation of respiration-correlated digital tomosynthesis in lung," Med. Phys. **37**(3), 1237–1245 (2010).
[31]J. C. Park *et al.*, "Four-dimensional cone-beam computed tomography and digital tomosynthesis reconstructions using respiratory signals extracted from transcutaneously inserted metal markers for liver SBRT," Med. Phys. **38**(2), 1028–1036 (2011).
[32]I. Vergalasova, J. Cai, and F. F. Yin, "A novel technique for markerless, self-sorted 4D-CBCT: Feasibility study," Med. Phys. **39**(3), 1442–1451 (2012).
[33]S. Kida *et al.*, "4D-CBCT reconstruction using MV portal imaging during volumetric modulated arc therapy," Radiother. Oncol. **100**(3), 380–385 (2011).
[34]W. P. Segars *et al.*, "Realistic CT simulation using the 4D XCAT phantom," Med. Phys. **35**(8), 3800–3808 (2008).
[35]B. Lu *et al.*, "A patient alignment solution for lung SBRT setups based on a deformable registration technique," Med. Phys. **39**(12), 7379–7389 (2012).
[36]G. W. Sherouse, K. Novins, and E. L. Chaney, "Computation of digitally reconstructed radiographs for use in radiotherapy treatment design," Int. J. Radiat. Oncol., Biol., Phys. **18**(3), 651–658 (1990).
[37]L. A. Feldkamp, L. C. Davis, and J. W. Kress, "Practical cone-beam algorithm," J. Opt. Soc. Am. A **1**(6), 612–619 (1984).
[38]J. P. Pluim, J. B. Maintz, and M. A. Viergever, "Mutual-information-based registration of medical images: A survey," IEEE Trans. Med. Imaging **22**(8), 986–1004 (2003).
[39]J. A. Nelder and R. Mead, "A simplex-method for function minimization," Comput. J. **7**(4), 308–313 (1965).
[40]X. Li *et al.*, "Use of simulated annealing for optimization of alignment parameters in limited MRI acquisition volumes of the brain," Med. Phys. **32**(7), 2363–2370 (2005).
[41]L. Ren *et al.*, "A novel digital tomosynthesis (DTS) reconstruction method using a deformation field map," Med. Phys. **35**(7), 3110–3115 (2008).
[42]L. Ren *et al.*, "Development and clinical evaluation of a three-dimensional cone-beam computed tomography estimation method using a deformation field map," Int. J. Radiat. Oncol., Biol., Phys. **82**(5), 1584–1593 (2012).
[43]A. Kavanagh *et al.*, "Obtaining breathing patterns from any sequential thoracic x-ray image set," Phys. Med. Biol. **54**(16), 4879–4888 (2009).
[44]J. H. Lewis *et al.*, "Markerless lung tumor tracking and trajectory reconstruction using rotational cone-beam projections: A feasibility study," Phys. Med. Biol. **55**(9), 2505–2522 (2010).
[45]S. S. Vedam *et al.*, "Acquiring a four-dimensional computed tomography dataset using an external respiratory signal," Phys. Med. Biol. **48**(1), 45–62 (2003).
[46]T. Kleshneva, J. Muzik, and M. Alber, "An algorithm for automatic determination of the respiratory phases in four-dimensional computed tomography," Phys. Med. Biol. **51**(16), N269–N276 (2006).
[47]H. Yan *et al.*, "The correlation evaluation of a tumor tracking system using multiple external markers," Med. Phys. **33**(11), 4073–4084 (2006).
[48]D. P. Gierga *et al.*, "The correlation between internal and external markers for abdominal tumors: Implications for respiratory gating," Int. J. Radiat. Oncol., Biol., Phys. **61**(5), 1551–1558 (2005).